

A COMPRESSION METHOD FOR 3-D LASER RANGE SCANS OF INDOOR ENVIRONMENTS BASED ON COMPRESSIVE SENSING

Oğuzcan Dobrucalı and Billur Barshan

Department of Electrical and Electronics Engineering, Bilkent University
06800, Bilkent, Ankara, Turkey

phone: (90-312) 290-2161, fax: (90-312) 266-4192, e-mail: {dobrucali, billur}@ee.bilkent.edu.tr
url: www.ee.bilkent.edu.tr

ABSTRACT

Modeling and representing 3-D environments require the transmission and storage of vast amount of measurements that need to be compressed efficiently. We propose a novel compression technique based on compressive sensing for 3-D range measurements that are found to be correlated with each other. The main issue here is finding a highly sparse representation of the range measurements, since they do not have highly sparse representations in common domains, such as the frequency domain. To solve this problem, we generate sparse innovations between consecutive range measurements along the axis of the sensor's motion. We obtain highly sparse innovations compared with other possible ones generated by estimation and filtering. Being a lossy technique, the proposed method performs reasonably well compared with widely used compression techniques.

1. INTRODUCTION

Many techniques have been developed for extracting the 3-D model of an environment that allow us to describe objects with undefined shapes or patterns [1]. Although using 3-D models are computationally expensive, they provide richer information than 2-D models, thus they are used in many fields varying from robot navigation [1] to art and architecture [2]. One approach in constructing 3-D models is using laser range finders that measure the range between the sensor and the objects within their field of view. The acquisition of the model is achieved by using either a conventional 3-D laser scanner, which is an expensive device, or a number of translating and/or rotating 2-D laser scanners [3].

In this study, we consider an indoor environment scanned in 3-D with a 2-D single laser range finder rotating around a horizontal axis above the ground level. The device used in this study is SICK LMS200, depicted in Figure 1(a), with maximum range 80 m, field of view 180°(Figure 1(b)), range resolution 1 mm, and angular resolution 0.5° [4]. This is the most widely used laser range finder in mobile robot applications today, both indoors and outdoors. Since the 3-D model is composed of a considerable number of 2-D scans that include a vast amount of measurements in total, the measurements should be compressed when they need to be transmitted or stored.

The *compression ratio* (CR), which is the ratio of the size of the compressed output to the size of the original data, the *distortion* (\mathcal{D}), which is the difference between the original data and its reconstruction, and the *speed* are the important criteria for measuring compression performance. In terms of the CR, an encoder is considered to be successful if it can reduce the size of the original data by more than one half, so

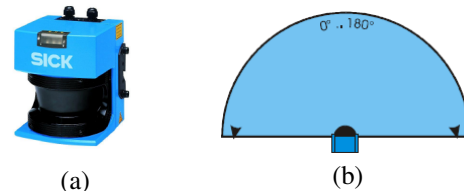


Figure 1: (a) SICK LMS200 and (b) its 180° field of view.

that the capacity of the communication channel or the storage medium is at least doubled for transmitting or storing the original data [5]. In this study, \mathcal{D} is measured as the root mean squared error (RMSE) between the original data and its reconstruction; and it should be sufficiently low for accurate compression.

The proposed method is capable of generating highly sparse representations for range measurement sequences as they are being acquired. These representations are then compressed based on *compressive sensing*. The method is similar to *difference encoding* and is a causal system. Therefore, it can compress even an infinite number of range measurement sequences, in theory.

The rest of this paper is organized as follows: Compressive sensing is reviewed in Section 2. The proposed method is described in Section 3 and compared with widely used compression techniques in Section 4. Conclusions and directions for future work are provided in the last section.

2. REVIEW OF COMPRESSIVE SENSING

Compressive sensing enables signals to be successfully reconstructed with fewer samples than Shannon/Nyquist sampling theorem requires. Unlike classical sampling, compressive sensing uses a linear sampling model with an optimization procedure for reconstructing the sampled signal [6].

The sampling model is composed of the *sparsifying basis* and the *measurement model* that satisfy *sparsity* and *incoherence* properties, respectively. Assume that the signals are represented by N samples, where N is very large. In the sparsifying domain Ψ , sparsity requires the signals to have sparse representations in which only a small number of the coefficients denoted by K will have large values, whereas the majority denoted by $(N - K)$ will be close to zero. For linear operations, Ψ can be chosen as an orthonormal basis denoted by $\Psi = [\psi_1, \dots, \psi_N]$ which is spanned by $\{\psi_i\}_{i=1}^N$. Thus, the sampled signal denoted by \mathbf{x} can be represented as $\mathbf{x} = \sum_{i=1}^N s_i \psi_i = \Psi \mathbf{s}$, where $\mathbf{s} = [s_1, \dots, s_N]^T$

in which $s_i = \langle \mathbf{x}, \boldsymbol{\psi}_i \rangle$. Notice that, \mathbf{x} and \mathbf{s} are different representations of the same signal in time and Ψ domains, respectively. The measurement model determines M measurements, where $M \ll N$, using a linear operator $\Phi = [\phi_1^T, \dots, \phi_M^T]^T$ composed of $\{\phi_i\}_{i=1}^M$, each of which is in \mathfrak{R}^N . The measurement model should be chosen so that $\{\phi_i\}_{i=1}^M$ cannot sparsely represent Ψ , which is a requirement of the incoherence property. Baraniuk suggests in [6] that the measurement model, in which each matrix element is chosen from a Gaussian distribution with zero mean and $\frac{1}{N}$ variance, is incoherent with any sparsifying basis with high probability. Given N and K , the lower bound on M is determined by:

$$M \geq cK \log \left(\frac{N}{K} \right) \quad (1)$$

where c is a small positive constant [6]. Eventually, the measurement vector denoted by $\mathbf{y} = [y_1, \dots, y_M]^T$, where $y_i = \langle \mathbf{x}, \phi_i \rangle$, is obtained such that $\mathbf{y} = \Phi \mathbf{x} = \Phi \Psi \mathbf{s} = \Theta \mathbf{s}$. The signal is then reconstructed at first by determining \mathbf{s} , given \mathbf{y} and Θ . Since Θ is $M \times N$ matrix with $M < N$, there is no unique solution to $\mathbf{y} = \Theta \mathbf{s}$. Therefore, the optimal solution is found by [7]:

$$\hat{\mathbf{s}} = \arg \min \|\tilde{\mathbf{s}}\|_1 \text{ such that } \mathbf{y} = \Theta \tilde{\mathbf{s}} \quad (2)$$

Finally, the original signal is approximated by $\hat{\mathbf{x}} = \Psi \hat{\mathbf{s}}$ with little distortion.

3. THE PROPOSED METHOD

Compressive sensing can be applied to compress any signal using a suitable sparsifying basis and an incoherent measurement model. Although forming the measurement model is a straightforward process, forming the sparsifying basis is a more challenging problem. The signals considered in this study are range measurement sequences taken within the sensor's field of view, as column vectors in \mathfrak{R}^N . Our aim is to find a representation of the signal which contains sufficiently sparse critical information to recover the signal with small error.

Two different experimental data sets [8] are used as benchmarks in this study. There are 29 and 82 3-D scans in the first and the second data set, respectively. Different features are observed in these scans as illustrated in Figure 2, where gray levels are directly proportional to the range measurements. Each 3-D scan is comprised of numerous 2-D scans that are sequentially acquired, while the sensor is rotated (in 471 and 225 steps for the first and the second data set, respectively) around a horizontal axis. Each 2-D scan is a range measurement vector in \mathfrak{R}^{361} (i.e., $N = 361$).

Before applying the sampling model described in Section 2, we seek possible sparse representations of the 2-D scans using well-known sparsifying bases. Thus, for the sample 3-D scan illustrated in Figure 2(a), we project the corresponding 2-D scans one at a time onto $N \times N$ sparsifying bases formed by using Fourier, Gabor, and Haar [9] dictionaries. The average percentages of the number of non-zero values to the total number of values in these projections are 74.7%, 61.3%, and 88.7%, respectively. To obtain more sparse representations, we attempted to sparsify the acquired range data by considering the innovations between:

- (i) two consecutive scans,
- (ii) each scan and its estimate using *linear regression* [10] based on the last two scans,

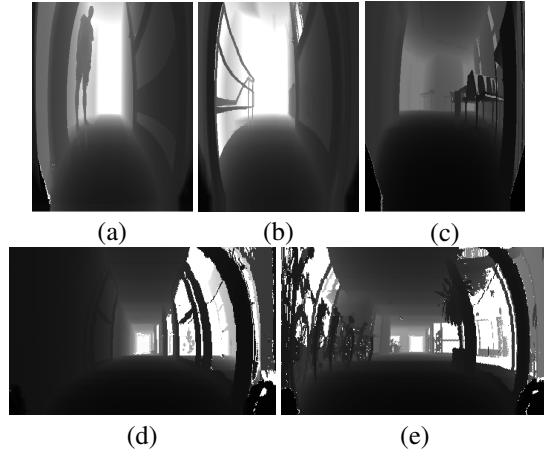


Figure 2: Sample 3-D scans from (a)–(c): the first and (d)–(e): the second data set.

- (iii) each scan and its estimate using a linear *Kalman filter* with the constant velocity kinematic state model [11],
- (iv) each scan and its estimate adding the previous scan to a difference estimate using a *2nd-order Wiener filter* [10],
- (v) each scan and its estimate adding the previous scan to a difference estimate using a 1-D random walk on the previous difference, such that $\mathbf{n}(t) = \alpha \mathbf{n}(t-1) + \mathbf{w}(t)$ where $\mathbf{n}(t)$ is the current difference at time t , α is correlation coefficient between consecutive differences, which is estimated as -0.4 by using all the scans in both data sets, and $\mathbf{w}(t)$ is white Gaussian noise.

The average percentages of the number of non-zero values to the total number of values in these innovations are 43.7%, 92.5%, 50.9%, 71.5%, and 27.3%, respectively.

Compared to the above percentages, the proposed method provides much more sparse innovations (6.5% for the same 3-D scan). The proposed method is composed of *encoder* and *decoder* modules, where the encoder consists of sparsifying, measurement, reconstruction stages, and the decoder involves only the reconstruction stage, as depicted in Figure 3. The sparsifying module generates sparse innovations for each scan, and the measurement module samples the innovations with the minimum number of samples. Finally, the reconstruction module rebuilds each scan from the samples encoded by the measurement module. The following subsections provide more detail on these three modules.

3.1 The Sparsifying Module

During the process of data acquisition, scans acquired consecutively have some similarities as well as differences. The differences may be caused by the motion of the sensor, as well as changes taking place in a dynamic environment. The sparsifying module uses the correlation between two scans acquired consecutively as the orientation of the sensor changes slightly. Because of the motion of the sensor, amplitude and phase differences between consecutive scans arise. Consequently, the sparsifying module generates an in-

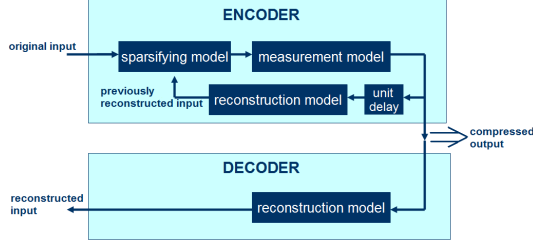


Figure 3: The operation scheme of the proposed method.

novation for the currently acquired n th scan \mathbf{r}_n by subtracting its approximation $\hat{\mathbf{r}}_n$ from itself. The module makes the reconstruction of the previously acquired scan \mathbf{r}_{n-1} similar to \mathbf{r}_n . At first, \mathbf{r}_{n-1} is generated at the encoder employing the reconstruction procedure the decoder follows. Then, $\hat{\mathbf{r}}_n$ is obtained by shifting \mathbf{r}_{n-1} along vertical and horizontal axes by amplitude (ε) and phase (δ) shifts, respectively.

Assume that the individual range measurements in \mathbf{r}_n and \mathbf{r}_{n-1} are denoted by $r_n[i]$ and $r_{n-1}[i]$, respectively, where $i = 1, 2, \dots, N$. We define an error function $\mathcal{E}^2 = \sum_{i=1}^N [r_n[i] - (r_{n-1}[i + \delta] + \varepsilon)]^2$ and set its partial derivatives with respect to ε and δ to zero to find the optimal values of ε and δ . Ignoring the δ term in $\frac{\partial \mathcal{E}^2}{\partial \varepsilon}$, ε becomes:

$$\varepsilon = \frac{1}{N} \sum_{i=1}^N (r_n[i] - r_{n-1}[i]) \quad (3)$$

where ε corresponds to the average amplitude difference between \mathbf{r}_n and \mathbf{r}_{n-1} . Since δ is assumed to be very small compared to N , $r_{n-1}[i + \delta]$ is expanded with the first two terms of its *Taylor series* expansion around i . Then, δ becomes:

$$\delta = \frac{\sum_{i=1}^N r'_{n-1}[i] (r_n[i] - r_{n-1}[i] - \varepsilon)}{\sum_{i=1}^N r'_{n-1}[i]^2} \quad (4)$$

where $r'_{n-1}[i]$ is the first-order derivative of \mathbf{r}_{n-1} at i .

After obtaining $\hat{\mathbf{r}}_n$, the difference sequence is computed as $\tilde{\mathbf{v}}_n = \mathbf{r}_n - \hat{\mathbf{r}}_n$, which is a sparse signal representing discontinuities in the scanned environment. If there is any remaining offset level in $\tilde{\mathbf{v}}_n$, $\tilde{\mathbf{v}}_n$ is further shifted to the zero level either in the positive or the negative vertical direction by the offset value Δ to improve the sparsity. Here, Δ is the most frequently appearing value in $\tilde{\mathbf{v}}_n$. After this step, we obtain a highly sparse innovation \mathbf{v}_n , such that 70% of the values in the representations are zero when we compress every 3-D scan in the first data set. It is shown in [12] that \mathbf{v}_n is a white sequence in time.

At the output of the sparsifying module, \mathbf{r}_n is represented with ε , δ , Δ , and \mathbf{v}_n . When \mathbf{r}_n and \mathbf{r}_{n-1} are highly correlated, such that the RMSE between \mathbf{r}_n and \mathbf{r}_{n-1} is less than an experimentally determined threshold (20 cm), \mathbf{v}_n becomes very small. If this is the case, \mathbf{r}_n is represented without \mathbf{v}_n . When \mathbf{r}_n and \mathbf{r}_{n-1} are not sufficiently correlated, such that the RMSE between \mathbf{r}_n and \mathbf{r}_{n-1} is larger than another experimentally determined threshold (200 cm), \mathbf{v}_n does not become a sparse signal, so \mathbf{r}_n is not encoded.

The performance of the sparsifying module is observed under additive white Gaussian noise with different standard deviations (σ). The 2-D scans from the 3-D scan illustrated

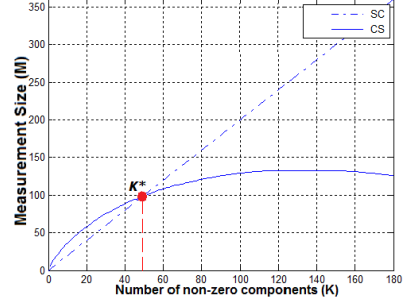


Figure 4: The measurement size M in SC and CS with respect to the number of non-zero components of a signal in \mathfrak{R}^{361} .

in Figure 2(a) are sparsified after adding zero mean white Gaussian noise with different standard deviations. When σ is up to 3 cm, the module can sparsify the scans as much as when the scans are not contaminated with noise. When σ is 10 cm, the average percentage of the number of non-zero values in \mathbf{v}_n to the total number of values in \mathbf{v}_n increases to 20%. When σ is greater than 10 cm, \mathbf{v}_n does not become sparse.

3.2 The Measurement Module

The measurement module obtains the minimum number of samples from \mathbf{v}_n by using either Simple Coding (SC) or Compressive Sampling (CS). SC encodes \mathbf{v}_n with the pairs of location and amplitude of the non-zero components. The measurement size (M), therefore, increases linearly as the number of non-zero components (K) increases. Despite this, the reconstruction error is zero when \mathbf{v}_n is rebuilt from the measurements taken with SC. CS measures arbitrary linear combinations of the components in \mathbf{v}_n as it is multiplied by the measurement model described in Section 2. In this case, M is determined using Equation (1) by assigning the value one to c . Furthermore, the resulting reconstruction error, which arises when \mathbf{v}_n is rebuilt from the measurements taken with CS, increases with K .

The measurement size M for the measurement vector \mathbf{m} taken using both SC and CS is illustrated in Figure 4. According to the figure, using SC seems to be advantageous over using CS in terms of M and the reconstruction error, when K is below the level indicated by K^* in the figure. Consequently, we apply SC when $K \leq K^*$, and apply CS, otherwise. We include a special character (i.e., π) at the beginning of \mathbf{m} when SC is applied, to inform the decoder about using SC instead of CS. Besides that, when $K > \frac{N}{2}$, \mathbf{v}_n cannot be considered as sparse, since the reconstruction error would be very high if \mathbf{v}_n were sampled using CS. In this case, \mathbf{r}_n is not encoded.

At the output of the measurement module, \mathbf{r}_n is represented with $\{\varepsilon, \delta, \Delta, \mathbf{m}\}$ if it is encoded. Otherwise, \mathbf{r}_n is left as it is.

3.3 The Reconstruction Module

The reconstruction module rebuilds \mathbf{r}_n from the output generated by the encoder. When \mathbf{r}_n is encoded, the output is composed of $\{\varepsilon, \delta, \Delta, \mathbf{m}\}$, and its length is $(M + 3)$ that is less than N . Otherwise, the output is \mathbf{r}_n with length N . Therefore, the reconstruction procedure starts with determining the length of the encoder output. If the length is N , the output is

stored directly as the reconstruction of \mathbf{r}_n . Otherwise, the output is decomposed into ε , δ , Δ , and \mathbf{m} . After this step, \mathbf{r}_{n-1} is shifted along the vertical and horizontal axes by ε and δ , respectively, to obtain $\hat{\mathbf{r}}_n$. Afterwards, \mathbf{v}_n is rebuilt from \mathbf{m} and Δ . In this step, if the first value of \mathbf{m} is π , then \mathbf{v}_n is rebuilt decoding the rest of \mathbf{m} with respect to the SC scheme, which involves filling an empty signal in \mathfrak{R}^N with the values of location and amplitude pairs given in the measurements. Otherwise, \mathbf{v}_n is rebuilt decoding \mathbf{m} with respect to the CS scheme, which involves solving Equation (2) by following the procedure in [7]. As soon as \mathbf{m} is decoded, the amplitude of \mathbf{v}_n is shifted by $-\Delta$ to obtain $\tilde{\mathbf{v}}_n$. Eventually, \mathbf{r}_n is reconstructed by adding $\tilde{\mathbf{v}}_n$ to $\hat{\mathbf{r}}_n$.

The reconstruction module is used at the decoder, as well as at the encoder to estimate the reconstructions generated by the decoder.

4. COMPARISON OF THE COMPRESSION PERFORMANCE OF THE PROPOSED METHOD WITH SOME OF THE WELL-KNOWN COMPRESSION TECHNIQUES

In this section, we compare the compression performance of the proposed method with some of the well-known and widely used lossless and lossy compression techniques that are applied to every 2-D scan independently in all of the 3-D scans in the data sets described in Section 3. Thus, for each technique in the comparison, we compare CR, \mathcal{D} , and the time required for encoding (t_{enc}) and decoding (t_{dec}). These values are calculated by averaging over the values obtained for the two data sets, separately.

We first compress the data sets using four of the lossless techniques, which are *Huffman*, *arithmetic*, *ZLIB*, and *GZIP* coding techniques. Huffman coding, which maps every character to distinct binary patterns based on the frequency of the appearance of the characters, is the optimal lossless coding technique. Similarly, arithmetic coding maps *blocks* of characters, instead of single characters, to distinct binary patterns based on the frequency of appearance of the blocks. Arithmetic coding is sometimes more efficient than Huffman coding, depending on the signal to be encoded [13]. ZLIB and GZIP are two popular compression techniques used in UNIX operating systems.

Besides lossless compression techniques, we apply two well-known lossy compression methods to the data sets. Since a 2-D scan can be considered as an image slice, we first apply JPEG compression [13]. Besides JPEG, 3-level *wavelet transform* using the *Haar dictionary* is applied to each 2-D scan, which is decomposed into six frequency components ranging from low to high frequencies. Only the lowest frequency components are used in reconstructing the scans. Finally, the data sets are encoded using the proposed method. In this method, small fluctuations in the compression performance are observed ($\pm 2\%$ in CR), since the measurement model in CS is determined arbitrarily in each trial. Therefore, CR, \mathcal{D} , t_{enc} , and t_{dec} are averaged, after the data sets are encoded 10 times using the proposed method.

The average compression performances of the methods described so far are summarized in Tables 1 and 2, for the first and the second data set, respectively. For the performances of the lossless methods, arithmetic coding can be considered to be efficient in terms of the CR for both data sets, however, it is slow compared to ZLIB and GZIP. On the other hand, these methods compress less than arithmetic

	method	CR (%)	\mathcal{D} (cm)	t_{enc} (s)	t_{dec} (s)
lossless	Huffman coding	41.7	0	165.6	610.6
	arithmetic coding	11.1	0	37.6	48.9
	ZLIB	65.3	0	0.4	0.2
	GZIP	76.7	0	0.5	0.3
lossy	JPEG	9.0	164.6	4.2	7.3
	3-level wavelet transform	12.7	37.3	0.8	0.9
	proposed method	10.9	12.9	15.3	14.5

Table 1: CR, \mathcal{D} , t_{enc} , and t_{dec} when the first data set is compressed by different lossless and lossy methods.

	method	CR (%)	\mathcal{D} (cm)	t_{enc} (s)	t_{dec} (s)
lossless	Huffman coding	683.3	0	101.8	363.1
	arithmetic coding	27.1	0	21.8	25.7
	ZLIB	140.8	0	0.3	0.1
	GZIP	143.8	0	0.3	0.2
lossy	JPEG	10.0	743.6	1.5	3.6
	3-level wavelet transform	12.7	353.8	0.5	0.5
	proposed method	32.0	4.8	1.9	1.7

Table 2: CR, \mathcal{D} , t_{enc} , and t_{dec} when the second data set is compressed with different lossless and lossy methods.

coding. For the performances of the lossy methods, JPEG and 3-level wavelet transform can be considered as fast and efficient techniques in terms of the CR, however they result in high distortions. When the proposed method is compared with the lossless methods considered here, the proposed method is faster than Huffman and arithmetic coding, but slower than ZLIB and GZIP. On the other hand, the proposed method compresses much more than ZLIB and GZIP. The performance of the proposed method is remarkable for the second data set that the lossless methods except arithmetic coding fail in compressing because the range of the values used in the second data set is broader than that of the first data set. When the proposed method is compared with the lossy methods, the proposed method is slower than the rest of the methods. However, it results in the least amount of distortion among them. For lossy compression, there always exists a trade-off between reducing the size of the input data, and minimizing the distortion on the reconstructions [13]. Consequently, being a lossy method, the proposed method provides a reasonably good compromise between the CR, accuracy of the reconstructions, and speed when its performance is compared with the performances of the well-known techniques considered in this study.

It is observed that the methods mentioned above compress the data sets at different rates because the complexity of the scenes in the second data set is higher, so the similarity between consecutive 2-D scans in the second data set is less than in the first. This is mathematically shown in [12] by computing average correlation coefficients between consecutive 2-D scans in the first and the second data sets. The performance of the proposed method is affected by this difference such that 57% of the 2-D scans in the first data set is encoded with $\{\varepsilon, \delta, \Delta\}$, whereas 64% of the 2-D scans in the second data set is not encoded. Therefore, the size of the first data set is reduced more than the size of the second data set. On the other hand, the error on the reconstructions of the first data set is larger than that of the second data set as illustrated in Figure 6, where gray levels are directly proportional to the

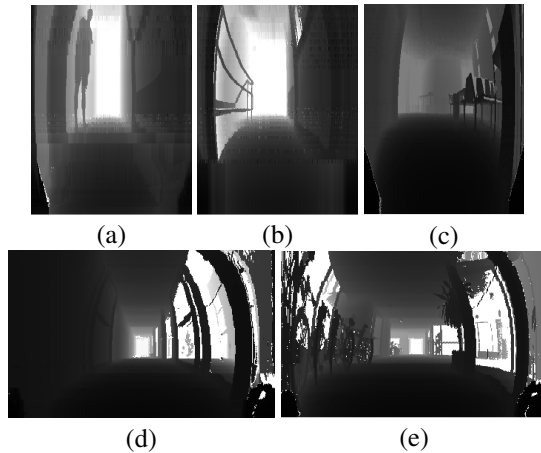


Figure 5: Reconstructions of the sample 3-D scans illustrated in Figure 2, respectively, using the proposed method.

amount of distortion.

In the literature, there are also some other compression techniques dedicated to 3-D range measurements. For instance, Kaushik and Xiao [14] encode 3-D scans with the union of planar patches fitted to the data. They achieve reducing the size of a 3-D scan comprised of 150,000 measurements by 94.65% within 18.67 s on the average.

5. CONCLUSION

In this study, we consider a 3-D model of an indoor environment acquiring with the commonly used SICK LMS200 laser range finder. The 2-D range scans forming the 3-D model are compressed as they are acquired, so that they can be stored or transmitted efficiently. From this perspective, we propose a compression technique based on compressive sensing, which focuses on sampling sparse signals efficiently, for sequentially acquired 2-D scans.

According to the criteria described in Section 1, the proposed method is fast and efficient in terms of the CR. Its performance seems reasonably acceptable compared with the performances of the well-known lossless and lossy methods considered in this paper. The proposed method is capable of compressing noisy scan data with a minimum SNR of 23 dB, which is also the limit for the proposed sparsifying module. The proposed method is recommended for applications where both the CR and speed are crucial. However, a lossless compression technique, such as arithmetic coding, can be used in applications where the accuracy of the range measurements is more important.

In summary, the proposed method provides acceptable CR among the compression techniques that we have considered, and as it provides a reasonably good balance between reconstruction accuracy and speed [13], it can be suitably used with 3-D scans. Our future work involves extending its application to other types of sequential measurements.

REFERENCES

- [1] C. Brenneke, O. Wulf, B. Wagner, "Using 3-D laser range data for SLAM in outdoor environments," *Proc. IEEE/RSJ Int. Conf. Intelligent Robots Syst.*, pp. 188–193, 2003.
- [2] M. Levoy, K. Pulli, B. Curless, S. Rusinkiewicz, D. Koller, L. Pereira, M. Ginzton, S. Anderson,

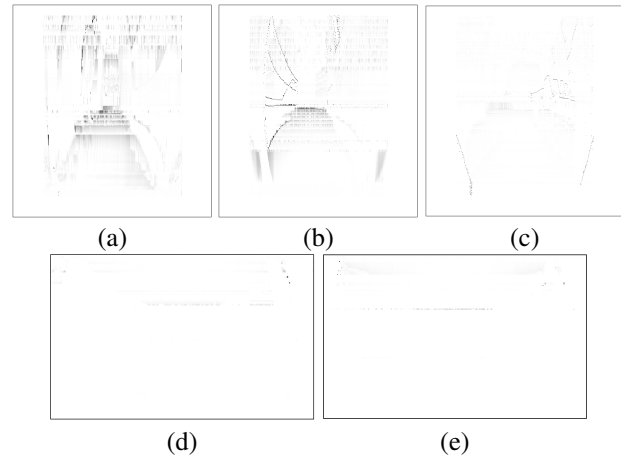


Figure 6: Illustrations of the error between the sample 3-D scans illustrated in Figure 2 and their reconstructions illustrated in Figure 5, respectively.

J. Davis, J. Ginsberg, J. Shade, D. Fulk, "The digital Michelangelo project: 3-D scanning of large statues," *Comput. Graphics Annual Conf.*, pp. 131–144, 2000.

- [3] D. Borrmann, J. Elseberg, K. Lingemann, A. Nüchter, J. Hertzberg, "Globally consistent 3-D mapping with scan matching," *Robot. Auton. Syst.*, 56(7): 130–142, 2007.
- [4] SICK AG, "Technical description, LMS 200/211/221/291 laser measurement systems," 2006.
- [5] D. Salamon, *A Guide to Data Compression Methods*, New York, U.S.A.: Springer, 2002.
- [6] R. G. Baraniuk, "Compressive sensing," *IEEE Signal Proc. Mag.*, 24(7): 118, 2007.
- [7] E. Candes, J. Romberg, "Signal recovery from random projections," *Proc. SPIE*, 5674: 76–86, 2005.
- [8] A. Nüchter, "Osnabrück University and Jacobs University knowledge-based systems research group repository," March 2010. <http://kos.informatik.uni-osnabrueck.de/3Dscans/> (10th and 15th data sets as of June 2011).
- [9] I. Daubechies, *Ten Lectures on Wavelets*, Philadelphia, Pennsylvania: Society for Industrial and Applied Mathematics, 1992.
- [10] M. H. Hayes, *Statistical Digital Signal Processing and Modeling*, U.S.A.: John Wiley & Sons, 1996.
- [11] Y. Bar-Shalom, T. E. Fortmann, *Tracking and Data Association*, San Diego, U.S.A.: Academic Press, 1988.
- [12] O. Dobrucali, *A Novel Compression Algorithm Based on Sparse Sampling of 3-D Laser Range Scans*, M.Sc. thesis, Bilkent University, Dept. of Electrical and Electronics Engineering, Ankara, Turkey, July 2010.
- [13] K. Sayood, *Introduction to Data Compression*, San Diego, U.S.A.: Academic Press, 2000.
- [14] R. Kaushik, J. Xiao, "Fast planar clustering and polygon extraction from noisy range images acquired in indoor environments," *Proc. IEEE Int. Conf. Mech. Autom.*, pp. 483–488, 2010.